METAL RICH RR LYRAE VARIABLES: I. THE EVOLUTIONARY SCENARIO

Giuseppe Bono
Osservatorio Astronomico di Trieste, Via G.B. Tiepolo 11, 34131 Trieste, Italy;
bono@oat.ts.astro.it

Filippina Caputo
Osservatorio Astronomico di Capodimonte, Via Moiariello 16, 80131 Napoli, Italy;
caputo@astrna.na.astro.it

Santi Cassisi [1]
Osservatorio Astronomico di Teramo, Via M. Maggini, 64100 Teramo, Italy;
cassisi@astrte.te.astro.it

Vittorio Castellani [2]
Dipartimento di Fisica, Università di Pisa, Piazza Torricelli 2, 56100 Pisa, Italy;
vittorio@astr1pi.difi.unipi.it

and

Marcella Marconi
Dipartimento di Fisica, Università di Pisa, Piazza Torricelli 2, 56100 Pisa, Italy;
marcella@astr1pi.difi.unipi.it

ABSTRACT

This paper presents evolutionary computations which investigate the theoretical predictions concerning metal rich RR Lyrae pulsators found both in the Galactic field and in the Galactic bulge. The main aim of this investigation is to provide a homogeneous evolutionary context for further analyses concerning the pulsational properties of these evolving structures. In this connection a suitable set of stellar models characterized by two different metal contents, namely Z=0.01 and Z=0.02 were followed through both H and He burning phases. This evolutionary scenario covers the theoretical expectations for pulsating He burning structures with ages ranging from 20 to less than 1 Gyr.

[1]Dipartimento di Fisica, Università de L'Aquila, Via Vetoio, 67100 L'Aquila, Italy

[2]Osservatorio Astronomico di Teramo, Via M. Maggini, 64100 Teramo, Italy

For each given assumption about the star metallicity we find that "old" He burning pulsators with ages larger than 2 Gyr have a common behavior, with Z=0.01 pulsators slightly more luminous and more massive than Z=0.02 pulsators. However, as soon as the metallicity increases above the solar value, the luminosity of Horizontal Branch (HB) stars increases again. This effect is a direct consequence of the expected simultaneous increase of both original He and metals.

The occurrence of "young" RR Lyrae pulsators is discussed, and we show that this peculiar group of variable stars can be produced if the mass loss pushes He burning stars originated from more massive progenitors into the instability region where electron degeneracy plays a minor role. In this case the luminosity of the pulsators could be substantially reduced with respect to the case of "old" variables, and therefore the theoretical expectations should also provide for this group of variable stars shorter pulsation periods.

Hydrogen burning isochrones for the quoted metallicity values are also presented and discussed.

Finally, the occurrence of a new "gravonuclear instability" in some HB models during the ignition of He shell burning is discussed. We have found that the appearance of this phenomenon is due to the opacity "bump" connected with Iron. At the same time we have also outlined the role that this feature could play on observables.

Subject headings: galaxies: stellar content – globular clusters: general – stars: evolution – stars: horizontal branch – stars: variables: other

1. INTRODUCTION

During the last decades RR Lyrae pulsators in galactic globular clusters (GGC) have been the object of lively debates and remarkable theoretical developments. However, it has long been known that metal poor globular cluster RR Lyrae are only a particular sample selected from a much larger population for RR Lyrae pulsators in the Galaxy. Preston (1959) was the first to draw attention to the group of metal rich RR Lyrae which constitute a significant component ($\sim 25\%$) of the RR Lyrae population in the solar neighborhood. In order to estimate the metal abundance of these objects he introduced the ΔS parameter, i.e. the ratio between the spectral type based on Hydrogen Balmer lines and the spectral type based on the Calcium K lines. Due to the dependence of this spectral index on the pulsation phase, Preston suggested evaluating the ΔS parameter at minimum light and pointed out, for the first time, that RR Lyrae stars located in the solar neighborhood present a metal rich ($0 < \Delta S < 2$) component, unknown in GGCs. At the same time this group of variable stars, in contrast with cluster variables, are also characterized by peculiar shorter periods.

Calibration of ΔS parameter in terms of [Fe/H] (Preston 1961; Butler 1975) has shown that this metal rich component reaches at least the solar metallicity, giving evidence for the occurrence of RR Lyrae variables well beyond the canonical range for halo population II stars. This observational evidence was further strengthened by Lub (1977), who presented an atlas of light and color curves in the Walraven VBLUW photometric system for 90 RR Lyrae in the southern field, which confirms the occurrence of a metal rich component reaching a solar-like composition. More recently, the investigation of a sample of 302 nearby RR Lyrae stars (Layden 1994,1995) has disclosed a metallicity distribution which peaks at $[Fe/H] \approx -1.5$, with a metal rich tail which extends to $[Fe/H] \approx 0$.

The peculiar periods of metal rich RR Lyrae represent a stimulating observational evidence to be connected with the evolutionary history of the pulsating structures. In a recent paper (Bono et al. 1996a and references therein) we have already shown that a nonlinear hydrodynamical approach to stellar pulsations can be connected with the prescriptions of stellar evolution for producing a theoretical scenario throwing light on several observed features of metal poor globular cluster variables. The investigation will now be extended to metal rich pulsators, testing the capability of the current theories to account for the observed peculiar pulsational behavior.

This paper deals with the results of an evolutionary investigation devoted to deriving a theoretical scenario for metal rich Galactic stellar populations. In a forthcoming paper (Bono et al. 1996b) we will finally approach theoretical expectations concerning metal rich pulsators, investigating the HR diagram location of the instability strip for both

fundamental and first overtone modes and discussing the pulsational properties of metal rich models at selected luminosity levels. On this basis theoretical expectations concerning the pulsational behavior of metal rich RR Lyrae will be eventually compared with available data.

2. LOW MASS STARS WITH SOLAR METALLICITY

According to a well-established scenario, RR Lyrae variables are unanimously recognized as HB stars which cross the instability strip during their central He burning evolutionary phase. In the case of globular clusters there is little doubt that RR Lyrae correspond to old He burning stars originated from Red Giant (RG) progenitors where electron degeneracy and neutrino cooling was efficient in the inner stellar structure during giant branch evolution. As a consequence, we expect that the mass of the He core at the He ignition and the luminosity of the Zero Age Horizontal Branch (ZAHB) are only marginally dependent on the assumed cluster age.

However, unlike globular cluster stars, we have no clear constraints about the age of field variable stars and, in turn, we cannot exclude the occurrence of younger and therefore originally more massive structures, with rather different He cores and He burning luminosities. As a consequence, in order to provide a sound approach to the theoretical predictions of metal rich He burning models, a preliminary evaluation of both the He core masses at the He ignition (M_{cHe}) and of the amount of extra helium (ΔY_{du}) dredged up during the RG (H shell burning) evolutionary phase as a function of the stellar age over a suitable range of ages is necessary.

For this purpose a detailed set of H burning models have been computed following their evolution from the Zero Age Main Sequence (ZAMS) until the Helium ignition for two different values of the stellar metallicity, namely Z=0.01 and Z=0.02. In this section we present the results concerning both H and He burning phases for stars with solar metallicity, i.e. Z=0.02, extending previous computations of He burning models already in the literature references for this metal abundance down to ages lower than 1 Gyr. The next section presents similar computations for Z=0.01. These new sequences of models allow for a straight-forward analysis of the evolutionary behavior of moderately metal rich stellar populations which represent a link with more metal poor stars, rarely debated in the literature.

Stellar models have been computed adopting the latest version of the FRANEC evolutionary code (see Chieffi & Straniero 1989), which includes several upgrades of the input physics.

Major improvements are the opacity tables for stellar interiors provided by Roger & Iglesias (1992) and low temperature molecular opacities for outer stellar layers by Alexander & Ferguson (1994). Both high and low temperature opacity tables assume Grevesse (1991) solar chemical mixture. Solar metallicity models assume an initial amount of Helium as given by $Y = 0.289$, whereas the mixing length parameter in the treatment of superadiabatic convective region has been taken equal to 2.25 times the local pressure scale height (H_p). According to the adopted physical inputs, these choices constrain the model with mass, chemical composition and age of the Sun to fit solar luminosity and effective temperature, producing the so-called Standard Solar Model. The adopted He abundance appears in good agreement with recent measurements of He abundance in the Galactic bulge which provide $Y = 0.28 \pm 0.02$ (Minniti 1995).

Table 1 gives selected evolutionary results for all the computed H burning models. The comparison of data in Table 1 with similar results already in the literature (Castellani, Chieffi & Straniero 1992; Horch, Demarque & Pinsonneault 1992; Dorman, Rood & O'Connell 1993; Bressan et al. 1993; Fagotto et al. 1994) shows reasonable agreement with marginal differences which scarcely affect the evolutionary scenario. However, this is not the case for the more massive models in Bressan et al. (1993) and Fagotto et al. (1994) in which the assumption of efficient core overshooting sensibly affects the evolution of the structures.

At the same time, the large number of evolutionary sequences computed until the Helium ignition allows for a detailed analysis of the "Red Giant Transition" (Sweigart, Greggio & Renzini 1989) for a stellar population with solar composition. Figure 1 shows the mass of the He core at the He ignition, the luminosity at the Red Giant Branch (RGB) tip and the age of the models as function of the mass of the evolving star. We find that the transition occurs at the age $t \simeq 8.9\ 10^8$ yrs, when at the tip of the RGB a star has $M \simeq 2.15 M_\odot$ and is characterized by a He core of $M_{cHe} \simeq 0.41 M_\odot$. For the sake of homogeneity with previous works (Sweigart et al. 1989; Sweigart, Greggio & Renzini 1990, hereinafter referred to as SGR; Cassisi & Castellani 1993), we have defined the transition mass M_{tr} as the stellar mass having a He core equal to the average value between the He core of degenerated structures and the absolute minimum in M_{cHe} at the He ignition. Comparison with previous results, as discussed in Cassisi & Castellani (1996), discloses that present results predict rather smaller transition masses (2.15 versus $2.6 M_\odot$) and therefore larger transition ages (900 versus 500 Myr) than expected in the pioneering paper by SGR but in agreement with previous computations by Castellani, Chieffi & Straniero (1992).

As a whole, present results confirm theoretical expectation that the age of low mass, metal rich RG stars, which experience strong electron degeneracy in the stellar core, can be much

lower in comparison with metal poor stars. As a consequence, at solar metallicity and for ages larger or of the order of 2.5 Gyr we expect a rather constant value for the mass of the He core at the He flash and, in turn, a common luminosity level for the ZAHB models.

These evolutionary results allow for the evaluation of updated H burning isochrones, which are presented in Figure 2 for selected assumptions about the stellar age. Table 2 summarizes the numerical data concerning the isochrones. This table reports in column (1) the stellar age (Gyr), in column (2) the mass value (solar units) of the model located at the Turn Off (TO) point, whereas in columns (3) and (4) are listed both the luminosity and the effective temperature of this point. Columns (5) and (6) present the V magnitude and the B-V color of the TO point, respectively. Theoretical observables have been transformed into the observational plane according to the bolometric corrections and to the color-temperature relations provided by Kurucz (1992). We adopted a bolometric magnitude for the Sun of $M_{Bol,\odot} = 4.75$ mag. The last column shows the V magnitude difference between the TO and the ZAHB models located at $\log T_e = 3.85$.

On the basis of these results the evolution of He burning models has been investigated for selected assumptions about the cluster ages, i.e. for different masses of the RGB progenitors constructed by assuming different evolutionary values for both M_{cHe} and ΔY_{du}. The stellar models selected as RGB progenitors have masses $M/M_\odot = 0.8, 1.0, 1.5, 2.0, 2.1$. The age of these models at the tip of the RGB ranges from 28.7×10^9 yrs down to 9.34×10^8 yrs. For each given age various efficiencies of mass loss during the RGB phase have been simulated by computing a set of He burning models with the total mass decreasing from the original value (no mass loss) down to, at least, 0.5 $M_\odot$. Figure 3 shows the evolutionary paths in the HR diagram for the "older" computed models, i.e. for models with progenitor masses smaller than or equal to $1.5M_\odot$, whereas Figure 4 shows the evolutionary path of HB stars with more massive progenitors. Table 3 reports the total stellar masses and the main evolutionary parameters of HB models for the two different assumptions on the chemical composition.

As expected, Figure 3 shows that for ages larger or of the order of 2.5 Gyr the effect of ages on HB evolutionary structure can be largely neglected. As discussed in the pioneering paper by Taam, Kraft & Suntzeff (1976), we find that when the metallicity is increased up to solar values the mass of ZAHB models at $\log T_e \simeq 3.85$, i.e. in the expected region where HB stars experience radial pulsation instability, decreases to about $0.5M_\odot$. However, our models show a larger luminosity ($\log L/L_\odot \simeq 1.52$ against 1.45) for the very simple reason that both our computations and the recent evaluations by Dorman et al. (1993) predict He core masses substantially larger than assumed in Taam et al. (1976, $M_{cHe} = 0.45M_\odot$). Figure 3 also shows that the adopted range of masses appears large enough to cover

the various different fates of low mass He burning stars, from the AGB manquè stars to structures that are massive enough to reach the thermal pulsating stage on the Asymptotic Giant Branch (AGB). The evolutionary properties of old He burning stellar models with solar metallicity have been exhaustively investigated in recent times (Brocato et al. 1990; Castellani & Tornambé 1991; Horch et al. 1992; Dorman et al. 1993), therefore the global characteristics are well known and they will not be discussed here. However, let us underline two remarkable features of the evolution which appear quite evident in Figure 3:

1) the location of the models along the ZAHB critically depends on the envelope mass, so that a change in the envelope mass of only $0.03 - 0.04 M_{\odot}$ shifts the ZAHB location from the low temperature region ($\log T_e \simeq 3.75$) to the high temperature region ($\log T_e \simeq 4.20$) which is located well beyond the blue side of the instability strip for RR Lyrae stars. As a consequence, HB stellar models with a solar metallicity show, depending on the envelope mass, a *flip - flop* behavior concerning the location on the ZAHB. As already discussed by Horch et al. (1992) and by Dorman et al. (1993), this peculiarity is a distinctive feature of old stellar populations with metallicity equal to or larger than the solar value. This of course leaves a small probability for the occurrence of HB radial pulsators;

2) due to the enhanced efficiency of the H shell, during central He burning the H-rich outer layers are efficiently burned into He. As a result, at the central He exhaustion metal rich HB stars present thinner H-rich envelopes in comparison with metal poor stars. Therefore the range of masses which show the typical AGB-manqué morphology becomes larger (for example see Castellani et al. 1994).

As a relevant point, Figure 4 shows that below 2.5 Gyr the location of HB shows a non-negligible dependence on age assumptions. As matter of fact, if we take into account ages below 2.5 Gyr the mass of the He core becomes smaller. We consequently find that the luminosity level of the HB at $\log T_e = 3.85$ goes from $\log L/L_{\odot} \simeq 1.5$ for old (t $>$ 2.5 Gyr) stars down to $\log L/L_{\odot} \simeq 1.4$ for t=1.1 Gyr ($2.0 M_{\odot}$ progenitor) and to $\log L/L_{\odot} \simeq 1.3$ for t= 0.93 Gyr ($2.1 M_{\odot}$ progenitor). According to data listed in Figure 1, the minimum luminosity of He burning stars should be reached for a progenitor as massive as M$\simeq 2.3 M_{\odot}$, that is for He burning stars with ages of the order of 0.69 Gyr. Numerical computations show that in such a case we expect stellar mass values around $0.36 M_{\odot}$ and ZAHB luminosities of the order of $\log L/L_{\odot} \simeq 1.15$ for He burning stars located inside the instability strip ($\log T_e \simeq 3.85$). Following such a theoretical evidence, present models foresee that possible "young" RR Lyrae should be characterized by both significantly lower luminosities and hence also by corresponding shorter periods.

2.1. OCCURRENCE OF GRAVONUCLEAR INSTABILITIES

Figure 4 shows that at the onset of He shell burning some "young" models present the unexpected evidence of iterative runaways which cause a sudden change of the effective temperature and in turn of the AGB location of these models. Figure 5 shows that such an occurrence takes place only for less massive models which reach the AGB from hotter effective temperatures, whereas Figure 6 gives details of the time behavior of both the luminosity and effective temperature of the models during the runaway phase. The dynamics of these "gravonuclear instabilities" is shown in Figure 7, in which we report the time behavior of the various energy sources which rule the physical structure of these models. Exhaustion of central He is followed, as expected, by the temporary reignition of the H burning shell. The classical evolutionary scenario predicts at this time that the reignition of the H burning shell should be subsequently followed by the quiescent ignition of the He shell.

However, in the quoted models for the first time we find that the He shell ignition causes a sudden and quick expansion of the structure which switches off the nuclear energy sources located both in the H and He shells. As soon as the external layers of the stellar envelope reach their maximum outward excursion, the structure experiences a contraction phase which implies both an increase of the effective temperature and the reignition of the H burning shell at first and later of the He burning shell. At this time the models have already performed a closed path in the HR diagram, and as soon as the reignition of He burning shell takes place they repeat the previous process with remarkable regularity.

The physical mechanism which rules the loops performed by these models can be easily found in the large opacity of stellar envelopes characterized by solar metal content. In order to properly disentangle the effects introduced by metals on the envelope structure we have undertaken several numerical experiments by adopting an *ad hoc* metallicity distribution for the stellar layers located above the H burning shell. The models which present "gravonuclear loops" have been indeed stopped just before the ignition of the He shell, and the subsequent evolution has been computed by assuming, in the outermost regions located at temperatures lower than 10^6 K, the radiative opacity for a more metal poor mixture, namely Y=0.28 and Z=0.0001. The evolutionary tracks plotted in Fig. 8 undoubtedly show that "fictitious" track (dashed line), in contrast with standard track, does not experience the "gravonuclear loops" at the ignition of the He shell. Moreover, even though the two evolutionary sequences originate from a common initial condition the "fictitious" models evolve on a completely different path.

On the basis of this simple test we may conclude that the appearance of this phenomenon in young metal rich stars is mainly due to the large opacity of the metal rich mixture and

in particular to the "opacity bump" produced by Iron in the temperature region located close to 2×10^5 K and for densities lower than 10^{-7} grcm^{-3}. Moreover, it is worth noting that in this temperature-density range the main opacity source of the stellar envelope is given by the Iron "bump" i.e. the opacity peak due to this element is not only larger than the Helium peak but also than the Hydrogen peak. The reader interested in a detailed discussion concerning this opacity feature is referred to the thorough papers recently provided by Iglesias et al. (1995); Iglesias & Rogers (1996) and by Seaton et al. (1994).

Due to the large opacity, the energy produced by the ignition of He shell burning cannot be easily dissipated through the large opacity layers, producing an increase of the local temperature which further enhances the energy production. In this first stage the mechanism is quite similar to the He shell flash occurring in the normal thermal pulses of AGB structures during the phase of He shell reignition. However, in the present case the expansion of the structures eventually quenches the process since the decrease of both temperature and density rapidly switches off the burning shells. Thus the process starts again and we find that the stars experience a few tens of similar "gravonuclear loops" before approaching a quiet He shell burning phase. As shown in Figure 6, the stars spend about 5 million years repeatedly crossing the instability strip at two different luminosity levels, $\log L/L_\odot \simeq 1.7$ and 1.9 respectively. Such an occurrence produces a small but not negligible probability of observing similar "high luminosity" metal rich type II Cepheid variables in the field (for en extensive discussion concerning this group of variable stars see Diethelm 1985). In fact, the "young" HB model ($M/M_\odot$=0.50) which experiences the gravonuclear instability spends a time ranging from $\approx$ 13,000 yrs during the first loops to $\approx$ 17,000 yrs during the last ones inside the instability strip. These evolutionary times, when compared with the lifetime spent by this model in the phase of central He burning (t$\approx 1.9 \times 10^8$ yrs) provide a probability to detect a type II Cepheid which is roughly of the order of 10^{-4}. Therefore even though these radial pulsators are rare they could be properly identified in the huge photometric databases of variable stars recently collected by the microlensing experiments.

According to the above leading-term physical considerations, the more massive models which are located at lower effective temperatures do not experience a "gravonuclear instability" because the temperature gradient, due to the efficiency of convective transport, is smoothed out over the whole envelope. Therefore for these models the ignition of He shell burning takes place without the expansion of the external layers since the energy leakage through the envelope is governed by the convective motions.

As far as older models with larger He cores are concerned, the "gravonuclear loops" do not appear for a completely different reason. In fact, for these models the energy provided

by the ignition of He shell burning cannot supply the amount of energy necessary for the expansion of the envelope and hence for pushing an extended region of the stellar envelope in the temperature-density region where the opacities present the quoted "bump". Therefore for these models the key parameter which inhibits the appearance of the "gravonuclear instability" is the ratio between the total stellar mass and the envelope mass i.e. $q = M_{env}/M_{tot}$, where M_{env} is the amount of mass located above the H shell. In fact this parameter attains too large values for stellar models located in this region of the HR diagram. A more quantitative analysis concerning the appearance of this phenomenon and its dependence on astrophysical parameters such as metal content and the q values will be discussed in a forthcoming paper (Bono et al. 1996c).

Detailed information on the time evolution of He burning models is shown in Figures 9 and 10, in which the time behavior of stellar luminosities and effective temperatures for all the computed models are shown. As expected on very general grounds, "old" models with progenitors masses smaller than the RG transition mass (i.e. M$\leq$1.5 M$_\odot$) show quite similar central He burning lifetimes. The He burning lifetimes for younger models, characterized by larger values of the progenitor masses, increase following the decrease of the He core at the ignition of central He burning. The maximum He burning lifetime will be reached in correspondence of the minimum value of M_{cHe}, where models are expected to have comparable lifetimes in H and He burning phases. In Figure 9 we can further appreciate the unusual large lifetimes of the hotter, less massive models, which make these models good candidates for UV emission in metal rich stellar clusters (see for example Greggio & Renzini 1990; Dorman et al. 1993; Dorman, O'Connell & Rood 1995).

The results concerning He burning evolution can be finally combined with previous results for H burning stars to give the difference in luminosity between the HB and the main sequence TO as a function of the cluster age, as reported in Table 2.

3. LOW MASS STARS WITH A METAL CONTENT Z=0.01

As already discussed, in order to cover the metallicity which separates solar metallicity models from metal poor stellar models, the investigation has been extended to a low metal abundance, namely Z=0.01. Assuming that the amount of original He is proportional to the heavy element content, according to a Helium enrichment ratio $\Delta Y/\Delta Z \approx 3.0$, for these models we adopted Y=0.255. On the basis of the discussion given in the previous sections, H-burning models for selected values of the stellar mass have been followed up to the ignition of central He burning. The masses of the evolved models have been again chosen such as to cover the RG transition phase. The dependence of the He core mass on the

stellar mass at the ignition of central He is reported in Figure 1 so that a proper comparison with similar data but for solar metallicity can be easily made. As already known (SGR), we expect that the transition mass decreases as soon as the metallicity is decreased and/or the amount of original He is increased. The evidence that our Z=0.01 models undergo the transition at masses similar to the solar case suggests that the difference in the initial Helium abundance is counteracted by the variation in metallicity.

Selected data for H-burning models are reported in Table 4. Comparison between data in Table 4 and similar data given in Table 1 for the solar metallicity case shows that when the metallicity decreases from the solar case down to Z=0.01 the transition mass increases from $M_{tr} = 2.15 M_{\odot}$ to about $M_{tr} = 2.21 M_{\odot}$, whereas the transition age slightly decreases. Figure 11 shows a selected sample of H-burning isochrones covering the age range from 900 Myr to 20 Gyr. Numerical data concerning these isochrones are given in Table 5, in the same order and with the same content as already given in Table 2 for solar metallicity stars. For the given original chemical composition we find that "old" RG stars with electronically degenerate He cores ignite 3α reactions when the central He core has reached the mass $M_{cHe} \approx 0.485 M_{\odot}$ and the H-rich envelope has been enriched in Helium by $\Delta Y_{du} \simeq 0.02$. The amount of Helium dredged up slightly depends on the age of the giant at the He flash. It is noteworthy that the decrease in both Z and Y acts in the direction of increasing the core mass at the He flash, as suggested by the computations.

Structural parameters given by H burning evolution have been adopted to produce ZAHB models which have been further followed all along their He burning evolutionary phase. The evolutionary parameters adopted for these He burning models are listed in Table 3. Figure 12 shows the path in the HR diagram of selected models as originated from a $1.0 M_{\odot}$ progenitor, which can be regarded as representative of the common behavior of "old" He burning objects originated from RG stars with electronically degenerate cores. A glance at the evolutionary tracks plotted in this figure shows that the "gravonuclear loops" now appear at the end of the He shell burning phase. These models do not play any role for properly defining the physical structure of RR Lyrae variables since they are located well behind the first overtone blue edge and therefore they will not be discussed here further.

However, the location in the HR diagram of the models which experience the "gravonuclear instabilities" before approaching the White Dwarf cooling sequence presents an intriguing feature worth being discussed. In fact, Figure 12 shows that the occurrence of the "gravonuclear loops" takes place at an effective temperature higher than $\approx 25,000$ K. As a consequence this mechanism could provide useful constraints on the appearance of the UV upturn observed in elliptical galaxies (Ferguson et al. 1991; Ferguson 1995 and references therein) which is approximately located around the quoted value of effective temperature.

At the same time the occurrence of "gravonuclear instabilities" provides a plain physical justification for the plausible existence of a "critical metallicity" value, i.e. the metal abundance above which the HB morphology and in particular the evolution of hot HB and AGB manquè stars is influenced by this parameter (for a critical theoretical review see Greggio & Renzini 1990; Brocato et al. 1990; Dorman et al. 1995 and references therein). This region of the HR diagram should be investigated in more detail since it turns out that these evolutionary phases can provide important clues concerning the final fate of low mass stars.

Comparison with results given in the previous section discloses than in the case Z=0.01 the ZAHB location appears moderately more luminous than in the solar case. At $\log T_e = 3.85$ we find now $\log L/L_\odot = 1.55$ against $\log L/L_\odot = 1.52$ for Z=0.02. It turns out that such a difference is governed by the variation of the metal content, since the decrease in Y alone would produce fainter HB. These two evaluations of the ZAHB luminosity can be integrated with similar data computed with exactly the same evolutionary code and physical inputs but for lower metallicity by Cassisi & Salaris (1996 and references therein) to produce an updated evaluation of the ZAHB luminosity as a function of the metallicity covering the range from Z=0.0001 to Z=0.02. Numerical values concerning such a parameter are reported in Table 6 and are displayed in Figure 13, together with other evolutionary parameters relevant for He burning models.

As already discussed in Castellani, Chieffi & Pulone (1991 hereinafter referred to as CCP), we find that the relation $\log L(3.85)$ (i.e. the ZAHB luminosity at the effective temperature $\log T_e = 3.85$) versus $\log Z$ presents a rather constant slope in the interval Z=0.0001-0.001, whereas for metallicity larger than Z=0.001 the dependence of $\log L(3.85)$ on the metallicity progressively increases. Nevertheless, Figure 13 now shows that above Z=0.006 the quoted dependence decreases again. Comparison with similar data given in CCP but for a constant value of the original He (Y=0.23) convincingly demonstrates that such a feature must be regarded as an evidence of the fact that the increase in He connected with the increase in metallicity starts to play a relevant role in determining the ZAHB luminosity. On the basis of the assumed Helium enrichment ratio, we can therefore suspect that for even larger metallicities the increase in He will eventually dominate, reversing the dependence of the HB on the content of heavy elements. This hypothesis has been tested by computing selected stellar models with a metal abundance a factor of two larger than the solar one. The result, as reported in both Table 6 and figure 13, supports such an occurrence and shows that the ZAHB luminosity reaches a minimum for solar composition, whereas for metallicity larger than this value it presents an upturn.

Data concerning the ZAHB luminosity can be translated in absolute V magnitude according

to Kurucz's (1992) atmosphere models. On the basis of the data displayed in Figure 14, we find that the $\log L(3.85)$, in the lower metallicity range (Z= 0.0001 - 0.001), scales with metallicity according to the following relation:

$$M_V(3.85) = 0.16 \cdot \log Z + 1.19 \approx 0.16 \cdot [Fe/H] + 0.91$$

which appears in excellent agreement with observational estimate of the slope of this dependence as given by Walker (1992) and Carney, Storm & Jones (1992), i.e. $\Delta M_V = 0.15 \cdot \Delta[Fe/H]$ and with a zero point which appears intermediate between the values given in the two above quoted investigations. The same Figure shows that when the metallicity is increased up to values as large as 0.006, the linear relation connecting the extreme lower limit takes the form:

$$M_V(3.85) = 0.21 \cdot \log Z + 1.36 \approx 0.21 \cdot [Fe/H] + 1.00$$

with a much larger "mean" dependence of HB magnitudes on the metallicity, i.e. as large as $\Delta M_V = 0.21 \cdot \Delta[Fe/H]$. However, it is worth noting that the zero point of such relations depends on both the adopted bolometric corrections and the bolometric magnitude assumed for the Sun.

The effect of lowering the age below the time of the RG transition is shown in Figure 15, which presents the evolutionary paths of a He burning model originated from a progenitor of $2.0 M_\odot$ and hence for an age of about 0.98 Gyr. Inspection of this figure shows that the gravonuclear instabilities have now disappeared, following the decreased opacity of the stellar envelopes. Comparison with the HR diagram location of "old" He burning models for the same value of Z shows that again when the age becomes lower the HB stars can sensibly attain lower luminosities ($\log L/L_\odot \simeq 1.46$). Again the minimum luminosity will be reached in correspondence of the minimum value of M_{cHe}, namely for a mass $M \approx 2.3 M_\odot$ at the age ≈ 0.63 Gyr. Calculations show that in such a case at $\log T_e = 3.85$ we should find He burning models with mass value $M \approx 0.36 M_\odot$ and with ZAHB luminosity as low as $\log L(3.85) \simeq 1.16$.

4. DISCUSSION AND CONCLUSIONS

In this paper we have explored the theoretical scenario concerning the evolutionary status of metal rich RR Lyrae pulsators in order to make theoretical predictions about the astrophysical parameters governing the pulsation phenomenon, namely stellar mass and

luminosity. In order to provide a reliable and homogeneous scenario for these predictions, evolutionary computations covering both H and He burning phases have been presented for selected choices about the original mass of the evolving stars and for two different assumptions about the star metallicity, namely Z=0.01 and 0.02.

When dealing with "old" HB stars originated from RG progenitors with electronically degenerate stellar cores we find that above Z=0.006 the HB luminosity keeps decreasing when the metallicity increases, until it reaches a luminosity minimum at solar metallicity values. In more metal rich stars the increase in the original He abundance should dominate the evolution, increasing again the luminosity of HB structures. Due to the already known (CCP) nonlinear behavior of the ZAHB luminosity with the metallicity it turns out that the $M_V(HB) - [Fe/H]$ relations based on metal poor globular cluster stars (Carney, Storm & Jones 1992; Walker 1992; Sandage 1993) cannot be safely extrapolated at higher metallicities. As a consequence even though the absolute magnitude of RR Lyrae itself, which is characterized by a metal abundance close to the solar value, has been recently provided by the Hipparcos mission (Perryman et al. 1995) this firm observational constraint cannot be *tout court* adopted to infer the reliability of the quoted relations in the metal poor range.

The occurrence of "young" RR Lyrae pulsators can be produced if mass loss pushes into the instability region He burning stars originated from more massive progenitors in which electron degeneracy plays a reduced or a negligible role. In this case the luminosity of the pulsators could be substantially reduced with respect to the case of "old" variables, thus decreasing theoretical expectations on pulsational periods.

We have found an interesting new "gravonuclear instability" connected with the high opacity of metal rich stellar envelopes of HB stars. The appearance of this feature can be understood in terms of leading-term physical arguments and the role played by the Iron opacity bump. On the basis of both luminosity and temperature excursions experienced by the solar metallicity models during the "gravonuclear loops" we predict that pulsation properties of metal rich Type II Cepheids could provide useful clues concerning the appearance of this phenomenon. Moreover, we have found that the "gravonuclear loops" in HB models characterized by a metal content of Z=0.01 take place in a different region of the HR diagram in comparison with the solar metallicity models. In fact, for the former models the "gravonuclear instabilities" are located at both higher luminosities and higher effective temperatures. This new finding adds valuable pieces of information for understanding the UV upturn observed in elliptical galaxies and offers a coherent picture concerning the role played by a "critical metallicity" value on the evolution of hot HB stars.

This general evolutionary scenario is presented to allow for an extensive approach to the

pulsational properties of metal rich RR Lyrae stars, but also for disclosing the astrophysical parameters which govern the evolutionary properties of field stars belonging to both the Galactic bulge and the solar neighborhood.

It is a pleasure to thank B. Dorman for many stimulating and valuable discussions on the advanced evolutionary phases of low mass stars. We are also grateful to an anonymous referee for the pertinence of his/her comments regarding the content and the style of an early draft of this paper which improved its readability. This research has made use of NASA's Astrophysics Data System Abstract Service. This work was partially supported by MURST, CNR-GNA and ASI.

REFERENCES

Alexander, D. R., & Ferguson, J. W. 1994, ApJ, 437, 879

Bono, G., Caputo, F., Castellani V. & Marconi M. 1996a, A&AS, in press

Bono, G., et al. 1996b, to be submitted

Bono, G., et al. 1996c, in preparation

Bressan, A., Fagotto, F., Bertelli, G. & Chiosi, C. 1993, A&AS, 100, 647

Brocato, E., Matteucci, F., Mazzitelli, I., & Tornambé, A. 1990, ApJ, 349, 458

Fagotto, F., Bressan, A., Bertelli, G., & Chiosi, C. 1994, A&AS, 105, 39

Butler, D. 1975, ApJ, 200, 68

Carney, B. W., Storm, J. & Jones, R. V. 1992, ApJ, 386, 663

Cassisi, S., & Castellani, V. 1993, ApJS, 88, 509

Cassisi, S., & Castellani, V. 1996, in preparation

Cassisi, S., & Salaris, M. 1996, MNRAS, in press

Castellani, M., Castellani, V., Pulone, L., & Tornambé, A. 1994, A&A, 282, 771

Castellani, M., & Tornambé, A. 1991, ApJ, 381, 393

Castellani, V., Chieffi, A. & Pulone, L. 1991, ApJS, 76, 911 (CCP)

Castellani, V., Chieffi, A. & Straniero, O. 1992, ApJS, 78, 517

Chieffi, A., & Straniero, O. 1989, ApJS, 71, 47

Dorman, B., O'Connell, R. W. & Rood, R. T. 1995, ApJ, 442, 105

Dorman, B., Rood, R. T., & O'Connell, R. W. 1993, ApJ, 419, 596

Ferguson, H. C., et al. 1991, ApJ, 382, L69

Ferguson, H. C. 1995, in IAU Symp. 164, Stellar Populations, eds. P.C. Van Der Kruit & G. Gilmore (Dordrecht: Kluwer), 239

Greggio, L. & Renzini, A. 1990, ApJ, 364, 35

Grevesse, N. 1991, in IAU Symp. 145, Evolution of Stars: the Photospheric Abundance Connection, eds. G. Michaud & A. Tutukov (Dordrecht: Kluwer), 63

Horch, E., Demarque, P. & Pinsonneault, M. 1992, ApJ, 388, L53

Iglesias, C. A., Wilson, B. G., Rogers, F. J., Goldstein, W. H., Bar-Shalom, A. & Oreg, J. 1995, ApJ, 445, 855

Iglesias, C. A. & Rogers, F. J. 1996, ApJ, 464, 943

Kurucz, R. L. 1992, in IAU Symp. 149, The Stellar Populations of Galaxies, eds. B. Barbuy & A. Renzini (Dordrecht: Kluwer), 225

Layden, A. C. 1994, AJ, 108, 1016

Layden, A. C. 1995, AJ, 110, 2288

Lub, J. 1977, A&AS, 29, 345

Minniti, D. 1995, A&A, 300, 109

Perryman, M. A. C. et al. 1995, A&A, 304, 69

Preston, G. W. 1959, ApJ, 130, 507

Preston, G. W. 1961, ApJ, 134, 633

Rogers, F. J. & Iglesias, C. A. 1992, ApJ, 401, 361

Sandage, A. 1993, AJ, 106, 703

Seaton, M. J., Yuan, Y., Mihalas, D. & Pradhan, A. K. 1994, MNRAS, 266, 805

Sweigart, A., Greggio L. & Renzini, A. 1989, ApJS, 69, 911

Sweigart, A., Greggio L. & Renzini, A. 1990, ApJ, 364, 527 (SGR)

Taam, R. E., Kraft, R. P. & Suntzeff, N. 1976, ApJ, 207, 201

Walker, A. R. 1992, ApJ, 390, L81

5. Figure Captions

Fig. 1. Evolutionary parameter for structure at the He ignition as a function of the stellar mass. From the top to the bottom are plotted the stellar age, the luminosity and the mass of the He core.

Fig. 2. Theoretical isochrones for the H burning phases of solar metallicity structures, for the labeled assumptions about the cluster age. The time interval between consecutive isochrones is 1 Gyr, with the exception of the two isochrones corresponding to 0.9 Gyr and 1 Gyr respectively.

Fig. 3. Comparison of the evolutionary paths in the HR diagram of "old" He burning structures. The squares mark the ZAHB location of two models computed by adopting total stellar masses of $M/M_{\odot}$ =0.52 and 0.54 respectively, and a RG progenitor mass of $M/M_{\odot}$ =0.8. The stellar mass values of the progenitors and the He core masses are labeled. The total stellar masses adopted in each set of HB models are reported in Table 3.

Fig. 4. Evolutionary paths in the HR diagram of "young" He burning structures compared with similar paths but for "old" models. Symbols are the same as in Fig. 3. The stellar mass values of the progenitors and the He core masses are labeled. The total stellar masses adopted in each set of HB models are reported in Table 3.

Fig. 5. The evolutionary tracks for the two models which experience "gravonuclear" instabilities. For these models the mass of the progenitor is equal to $2.0M_{\odot}$.

Fig. 6. *Top panel*: The time behavior of the surface luminosity and effective temperature during the "gravonuclear loops" of the $0.50M_{\odot}$ model. *Bottom panel*: same as top panel but referred to the $0.49M_{\odot}$ model.

Fig. 7. Time behavior of the gravitational luminosity (em panel a), of the hydrogen (*panel b*) and helium (*panel c*) luminosities during the "gravonuclear loops" for the $0.50M_{\odot}$ model.

Fig. 8. Comparison between the standard evolutionary track (solid line) and the "fictitious" sequence of models (dashed line) constructed by adopting for the stellar layers located above the H burning shell ($T \leq 10^6$ K) the radiative opacities of a "fictitious" metal poor (Y=0.28, Z=0.0001) mixture. The circle marks the evolutionary phase which precedes

the ignition of the He shell burning. See text for further explanation.

Fig. 9. Time behavior of the luminosity for all He burning models with solar metallicity. Physical parameters are labeled.

Fig. 10. Time behavior of the effective temperature for all He burning models with solar metallicity. Physical parameters are labeled.

Fig. 11. Same as Figure 2, but referred to a different chemical composition, namely Z=0.01 and Y=0.255.

Fig. 12. Evolutionary path in the HR diagram of selected He burning models computed by assuming a progenitor mass value of $M = 1.0 M_{\odot}$ and a metallicity Z=0.01. The He core mass is labeled, whereas the total stellar masses adopted are reported in Table 3.

Fig. 13. *Panel a*: Helium abundance in the envelope as a function of metallicity for the $M = 0.8 M_{\odot}$ model at the RGB tip. The adopted initial Helium abundance -dashed line- is also shown. *Panel b*: the mass of the He core at the He burning ignition for the same model, whereas *panel c* shows the luminosity of the ZAHB at the effective temperature $\log T_e = 3.85$ for an "old" Red Giant progenitor. See text for further explanation.

Fig. 14. The V magnitude of ZAHB at $\log T_e = 3.85$ as a function of metallicity for an "old" Red Giant progenitor. The bolometric corrections given by Kurucz (1992) have been used. We also adopted a bolometric magnitude for the Sun equal to 4.75 mag.

Fig. 15. Same as as Figure 12, but the evolutionary tracks have been constructed by assuming an initial mass value for the progenitor equal to $2.0 M_{\odot}$. In order to avoid crowding problems the evolutionary paths located at the higher temperatures have been plotted by adopting dotted and dashed lines. The He core mass is labeled, whereas the total stellar masses adopted are reported in Table 3.

Table 1. Selected theoretical evolutionary quantities for the models with solar metallicity.

$M/M_{\odot}$[a]	$\log(L/L_{\odot})_{tip}$[b]	$\log t_{He}$[c]	M_{cHe}[d]	ΔY_{du}[e]
0.8	3.442	10.458	0.479	0.017
1.0	3.439	10.095	0.478	0.021
1.2	3.434	9.804	0.477	0.019
1.4	3.433	9.565	0.477	0.016
1.5	3.433	9.462	0.476	0.014
1.6	3.430	9.363	0.476	0.013
1.8	3.392	9.185	0.469	0.010
2.0	3.255	9.036	0.445	0.009
2.1	3.128	8.970	0.425	0.007
2.3	2.393	8.840	0.339	0.011
2.4	2.473	8.785	0.342	0.011
2.5	2.487	8.733	0.345	0.012
3.0	2.587	8.509	0.391	0.015

[a]Stellar mass value (solar units).

[b]Logarithmic luminosity (solar units) at the RGB tip.

[c]Logarithmic age (yrs) at the RGB tip.

[d]Mass value of the He core (solar units) at the He ignition.

[e]Amount of extra-helium dredged up during RGB evolution

Table 2. Selected evolutionary data concerning the solar metallicity isochrones.

Age (Gyr)	$M/M_{\odot}$[a]	$\log(L/L_{\odot})$[b]	$\log T_e$[c]	M_V[d]	$(B-V)$[e]	ΔV_{HB}^{TO}[f]
0.9	2.049	1.500	3.910	1.080	0.139	-0.39
1.0	1.976	1.435	3.899	1.233	0.177	-0.15
2.0	1.566	1.018	3.835	2.307	0.390	1.29
3.0	1.372	0.779	3.815	2.922	0.461	1.95
4.0	1.255	0.606	3.802	3.367	0.510	2.39
5.0	1.173	0.472	3.791	3.714	0.553	2.74
6.0	1.118	0.385	3.782	3.944	0.588	2.97
7.0	1.072	0.316	3.775	4.127	0.616	3.15
8.0	1.050	0.275	3.770	4.237	0.637	3.26
9.0	1.020	0.240	3.766	4.332	0.653	3.36
10.0	0.996	0.203	3.762	4.432	0.669	3.46
11.0	0.975	0.170	3.758	4.523	0.686	3.55
12.0	0.949	0.140	3.754	4.606	0.703	3.63
13.0	0.930	0.112	3.750	4.685	0.719	3.72
14.0	0.916	0.089	3.747	4.750	0.732	3.78
15.0	0.902	0.072	3.744	4.800	0.744	3.82
16.0	0.891	0.058	3.742	4.840	0.752	3.87
17.0	0.880	0.049	3.739	4.871	0.765	3.90
18.0	0.870	0.037	3.736	4.909	0.777	3.93
19.0	0.858	0.025	3.734	4.945	0.785	3.97
20.0	0.847	0.010	3.732	4.989	0.793	4.02

[a]Mass value at the TO point (solar units).

[b]Logarithmic luminosity of the TO point (solar units).

[c]Logarithmic effective temperature (K) of the TO point.

[d]V Magnitude of the TO point (mag).

[e]B-V color of the TO point (mag).

[f]V Magnitude difference between the TO point and the ZAHB at $\log T_e = 3.85$.

Table 3. Selected evolutionary parameters for the He burning phase for different assumptions on chemical composition and RG progenitor masses.

M_{pr} [a]	Y_{HB} [b]	M_{cHe} [c]	M_{tot} [d]
		Z=0.02 $Y_{ZAMS} = 0.289$	
0.8	0.306	0.479	0.490, 0.500, 0.510, 0.520, 0.530, 0.540 0.550, 0.600, 0.650, 0.700, 0.750, 0.800
1.0	0.310	0.478	0.490, 0.500, 0.550, 0.600, 0.650, 0.700 0.750, 0.800, 0.850, 0.900, 0.950, 1.000
1.5	0.303	0.477	0.500, 0.550, 0.600, 0.650, 0.700, 0.750 0.800, 0.900, 1.000, 1.100, 1.200, 1.300 1.400, 1.500
2.0	0.298	0.445	0.490, 0.500, 0.510, 0.520, 0.550, 0.600 0.900, 1.000, 1.200, 1.300, 1.400, 1.500 1.600, 1,800, 1.900, 2.000
2.1	0.296	0.425	0.500, 1.000, 1.200, 1.400, 1.600, 1.800 2.000, 2.100
		Z=0.01 $Y_{ZAMS} = 0.255$	
1.0	0.277	0.487	0.495, 0.500, 0.510, 0.520, 0.530, 0.540 0.550, 0.560, 0.570, 0.580, 0.590, 0.600 0.630, 0.650, 0.700, 0.750, 0.800, 0.900 1.000
2.0	0.266	0.464	0.465, 0.470, 0.475, 0.480, 0.490, 0.500 0.510, 0.520, 0.530, 0.540, 0.550, 0.580 0.600, 0.700, 0.800, 1.000, 1.200, 1.600 1.800, 2.000

[a] Stellar mass value for the RG progenitor (solar units). [b] Helium abundance adopted for HB models. [c] Helium core mass value (solar units). [d] Total stellar mass value adopted for HB models (solar units).

Table 4. Same as Table 1 but the data are referred to a different chemical composition: Z=0.01 and Y=0.255.

$M/M_{\odot}$	$\log(L/L_{\odot})_{tip}$	$\log t_{He}$	M_{cHe}	ΔY_{du}
0.8	3.447	10.402	0.489	0.017
1.0	3.442	10.038	0.487	0.022
1.2	3.438	9.745	0.485	0.023
1.5	3.435	9.410	0.485	0.017
1.6	3.434	9.315	0.485	0.015
1.8	3.418	9.140	0.482	0.012
2.0	3.323	8.991	0.464	0.011
2.2	3.088	8.866	0.426	0.012
2.3	2.434	8.798	0.331	0.013
2.5	2.499	8.695	0.341	0.014
3.0	2.562	8.481	0.381	0.017

Table 5. Same as Table 2 but the data are referred to a different chemical composition: Z=0.01 and Y=0.255.

Age	$M/M_\odot$	$\log(L/L_\odot)$	$\log T_e$	M_V	$(B-V)$	ΔV_{HB}^{TO}
0.9	1.748	1.144	3.903	1.993	0.175	0.82
1.0	1.686	1.081	3.892	2.149	0.204	0.98
2.0	1.490	1.012	3.863	2.333	0.293	1.39
3.0	1.297	0.736	3.834	3.043	0.379	2.10
4.0	1.184	0.561	3.814	3.496	0.441	2.55
5.0	1.129	0.489	3.804	3.683	0.477	2.74
6.0	1.085	0.432	3.796	3.833	0.504	2.89
7.0	1.047	0.379	3.790	3.971	0.526	3.03
8.0	1.016	0.338	3.785	4.079	0.545	3.14
9.0	0.990	0.306	3.781	4.164	0.562	3.22
10.0	0.965	0.272	3.776	4.256	0.579	3.31
11.0	0.944	0.243	3.772	4.332	0.594	3.39
12.0	0.925	0.218	3.768	4.401	0.609	3.46
13.0	0.908	0.194	3.765	4.465	0.622	3.52
14.0	0.890	0.163	3.762	4.549	0.635	3.61
15.0	0.876	0.143	3.759	4.604	0.646	3.66
16.0	0.862	0.116	3.756	4.676	0.657	3.73
17.0	0.849	0.091	3.754	4.744	0.667	3.80
18.0	0.837	0.068	3.751	4.806	0.677	3.87
19.0	0.827	0.054	3.749	4.846	0.685	3.91
20.0	0.817	0.034	3.747	4.902	0.694	3.96

Table 6. Selected evolutionary parameters at the RGB tip and at the ZAHB for different assumptions concerning the metallicity. All data are referred to an "old" cluster population.

Z[a]	Y_{ZAMS}[b]	Y_{ZAHB}[c]	M_{cHe}[d]	$\log L(3.85)$[e]	$M(3.85)/M_{\odot}$[f]	M_V^{ZAHB}[g]
0.0001	0.230	0.238	0.511	1.735	0.796	0.557
0.0003	0.230	0.240	0.507	1.699	0.711	0.636
0.0006	0.230	0.242	0.504	1.678	0.671	0.679
0.0010	0.230	0.243	0.502	1.661	0.648	0.715
0.0030	0.230	0.245	0.498	1.610	0.608	0.823
0.0060	0.230	0.246	0.495	1.556	0.585	0.941
0.0100	0.255	0.272	0.489	1.542	0.575	0.962
0.0200	0.289	0.306	0.479	1.523	0.545	0.973
0.0400	0.340	0.357	0.468	1.533	0.540	0.938

[a]Metal content.

[b]Initial He abundance on the Zero Age Main Sequence.

[c]He abundance in the envelope of the ZAHB models.

[d]Mass value of He core at the RGB tip (solar units).

[e]Logarithmic ZAHB luminosity taken at $\log T_e = 3.85$.

[f]Mass value of the ZAHB model located at $\log T_e = 3.85$.

[g]V magnitude of the ZAHB.

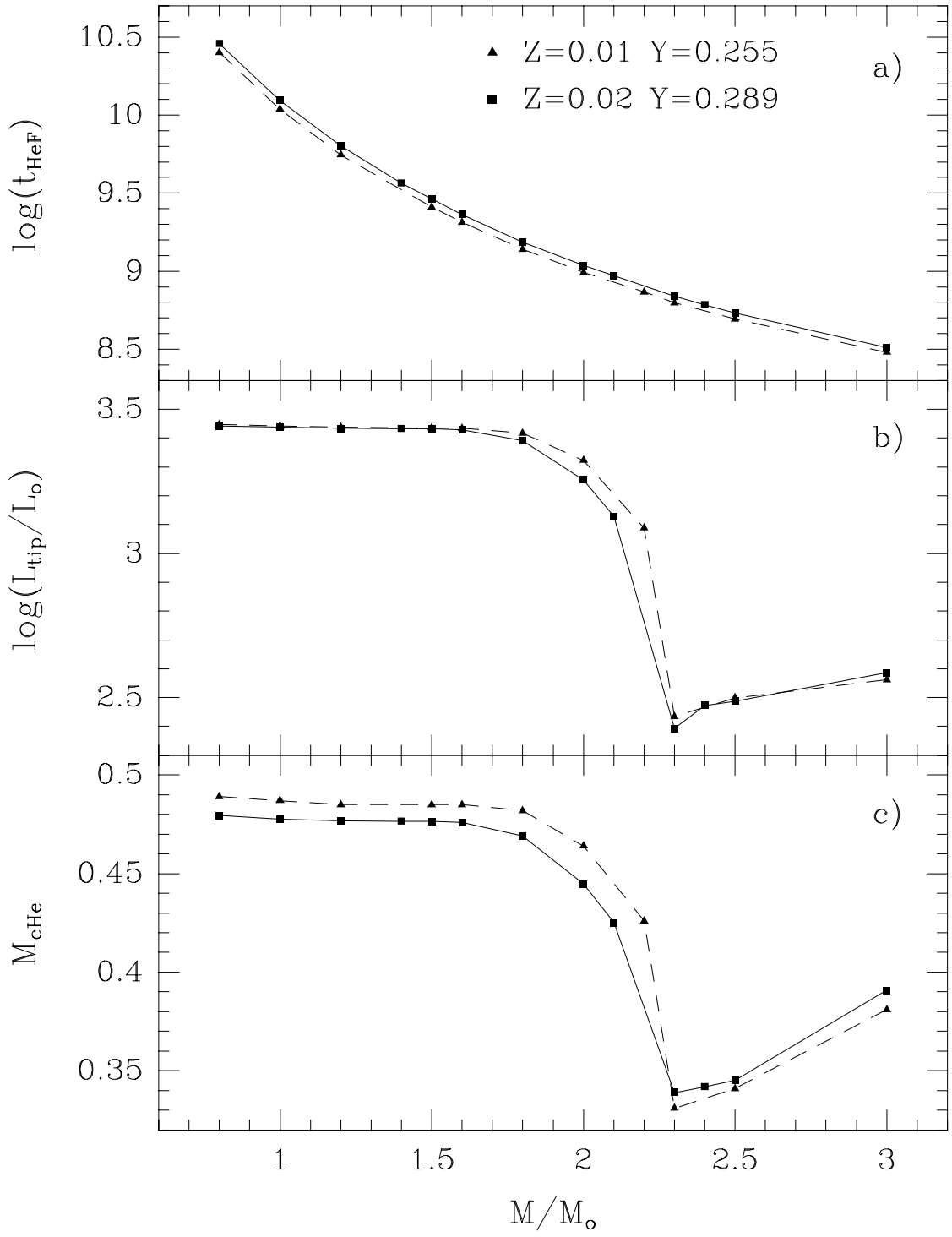
Z=0.01 Y=0.255
Z=0.02 Y=0.289
a)
b)
c)
log(t_HeF)
log(L_tip/L_o)
M_cHe
M/M_o
10.5
10
9.5
9
8.5
3.5
3
2.5
0.5
0.45
0.4
0.35
1
1.5
2
2.5
3

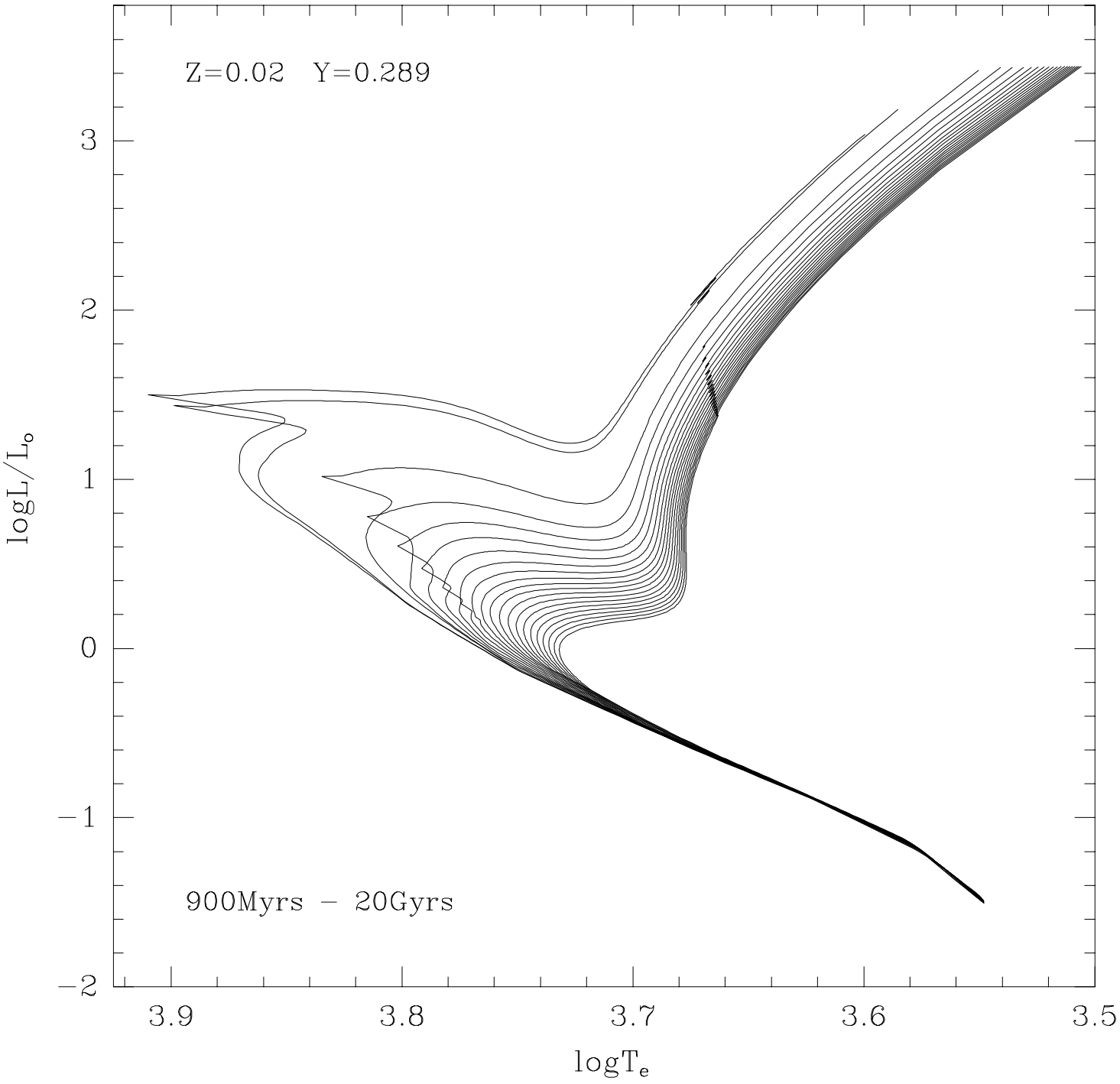
Z=0.02 Y=0.289
900Myrs – 20Gyrs
3
2
1
0
−1
−2
logL/L$_o$
3.9
3.8
3.7
3.6
3.5
logT$_e$

This figure "fig3.gif" is available in "gif" format from:

http://arXiv.org/ps/astro-ph/9609153v2

This figure "fig4.gif" is available in "gif" format from:

http://arXiv.org/ps/astro-ph/9609153v2

This figure "fig5.gif" is available in "gif" format from:

http://arXiv.org/ps/astro-ph/9609153v2

This figure "fig6.gif" is available in "gif" format from:

http://arXiv.org/ps/astro-ph/9609153v2

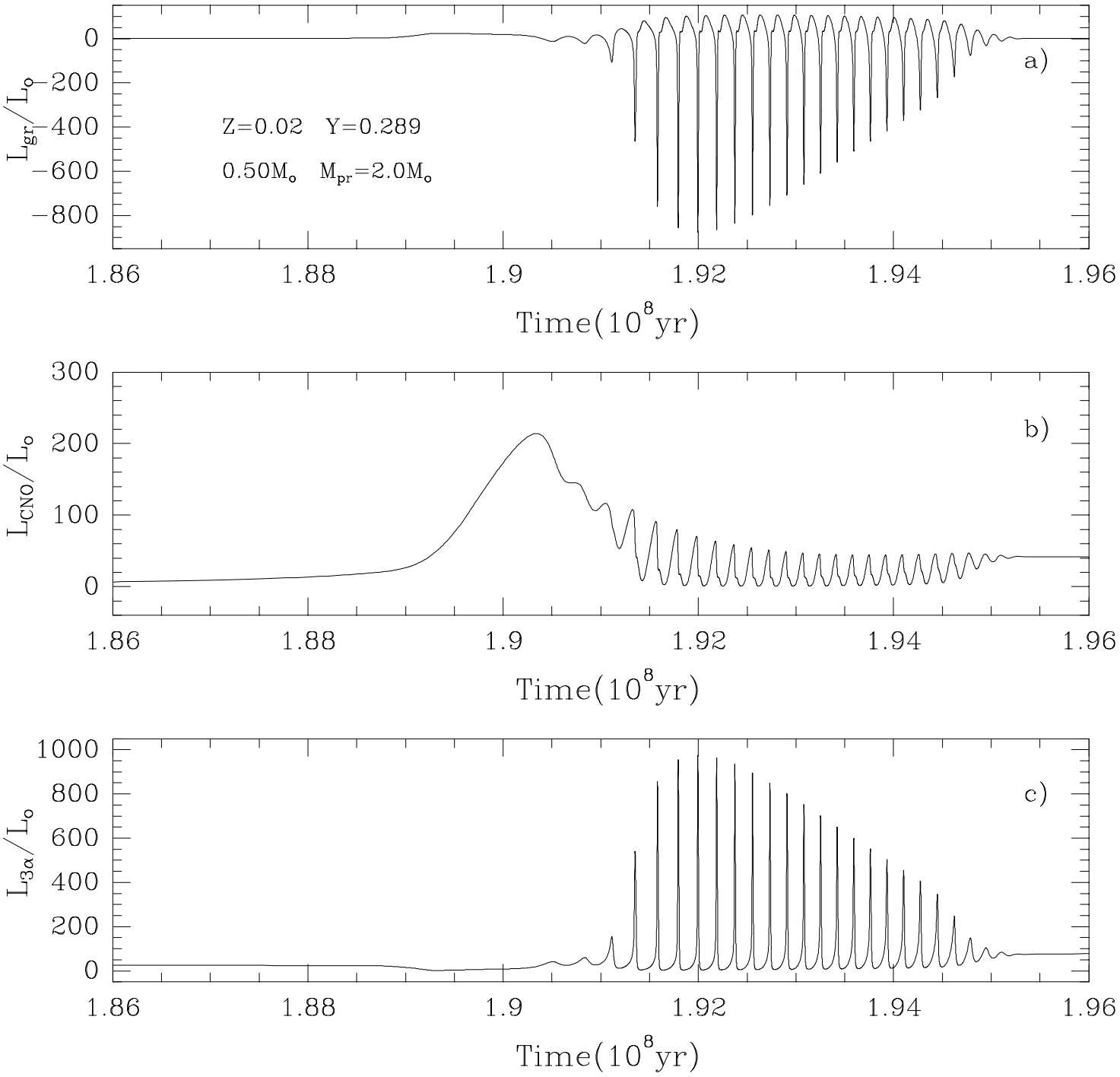
a)
Z=0.02 Y=0.289
0.50M$_o$ M$_{pr}$=2.0M$_o$
L$_{gr}$/L$_o$
0
−200
−400
−600
−800
1.86
1.88
1.9
1.92
1.94
1.96
Time(10^{8}yr)
b)
L$_{CNO}$/L$_o$
300
200
100
0
1.86
1.88
1.9
1.92
1.94
1.96
Time(10^{8}yr)
c)
L$_{3\alpha}$/L$_o$
1000
800
600
400
200
0
1.86
1.88
1.9
1.92
1.94
1.96
Time(10^{8}yr)

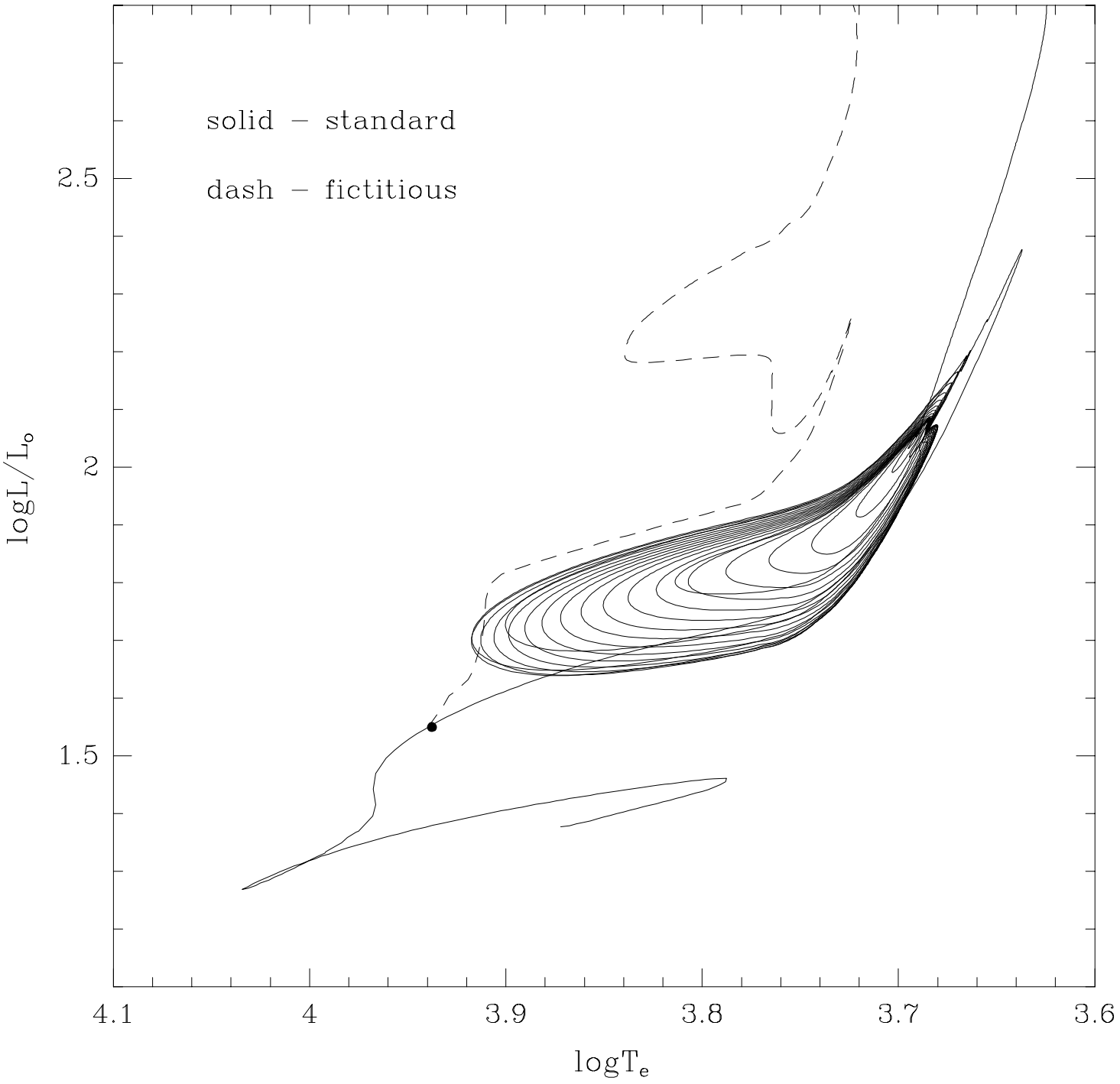
solid – standard
dash – fictitious
2.5
2
1.5
logL/L$_o$
4.1
4
3.9
3.8
3.7
3.6
logT$_e$

This figure "fig9.gif" is available in "gif" format from:

http://arXiv.org/ps/astro-ph/9609153v2

This figure "fig10.gif" is available in "gif" format from:

http://arXiv.org/ps/astro-ph/9609153v2

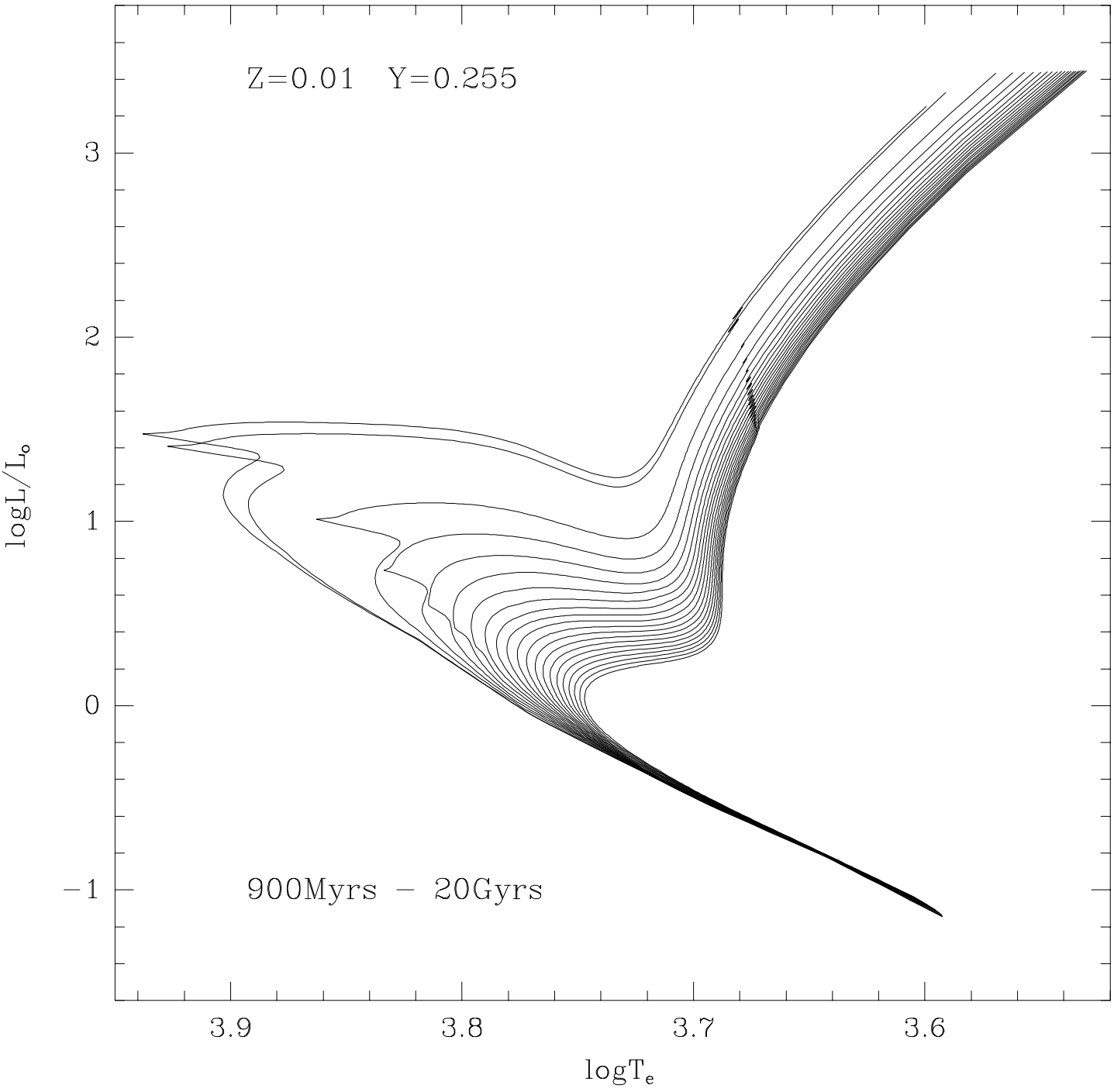
Z=0.01 Y=0.255
900Myrs – 20Gyrs
3
2
1
0
−1
3.9
3.8
3.7
3.6
logL/L$_o$
logT$_e$

This figure "fig12.gif" is available in "gif" format from:

http://arXiv.org/ps/astro-ph/9609153v2

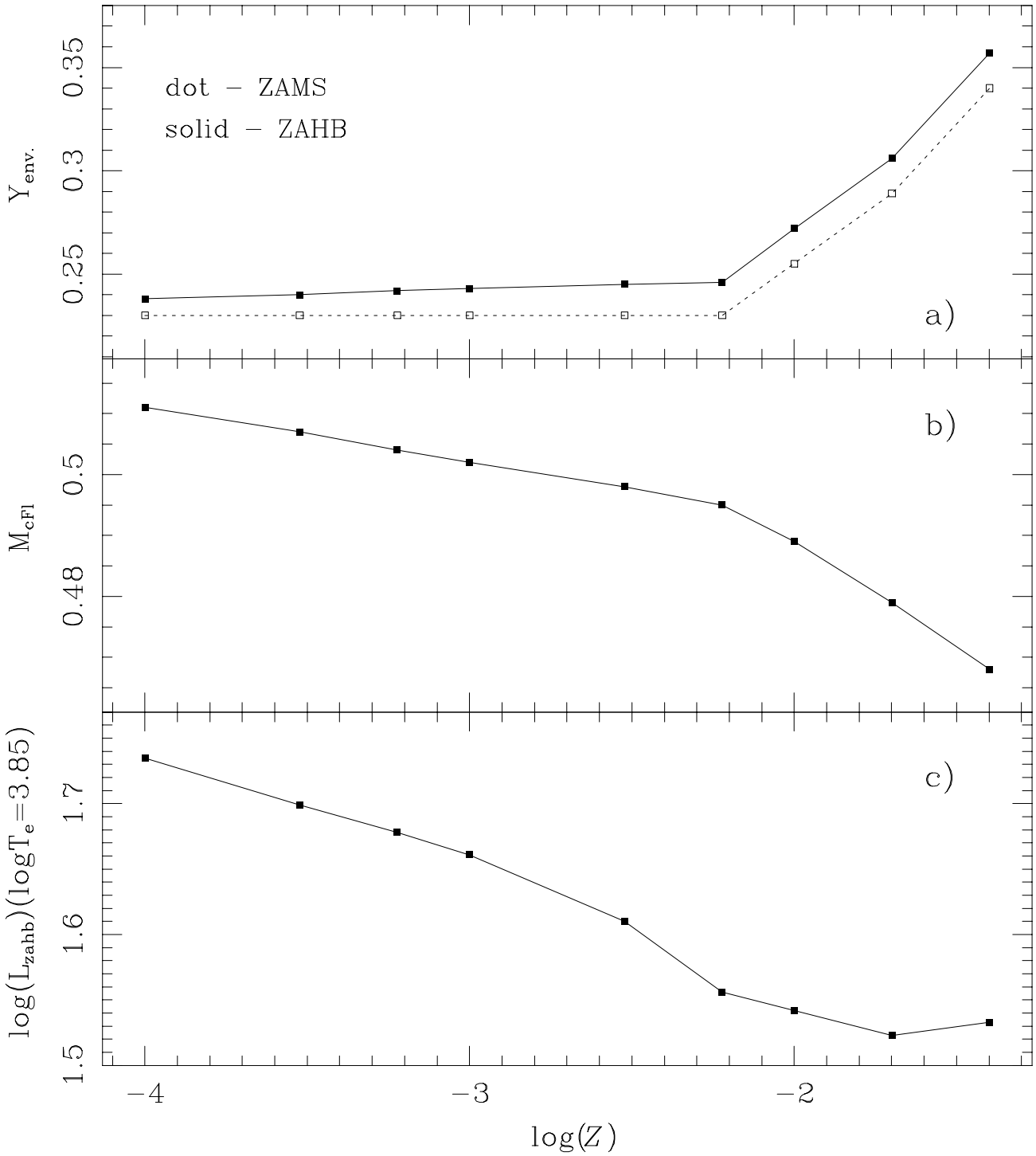
dot – ZAMS
solid – ZAHB
a)
b)
c)
$Y_{env.}$
M_{cFl}
$\log(L_{zahb})(\log T_e=3.85)$
0.25
0.3
0.35
0.48
0.5
1.5
1.6
1.7
−4
−3
−2
log(Z)

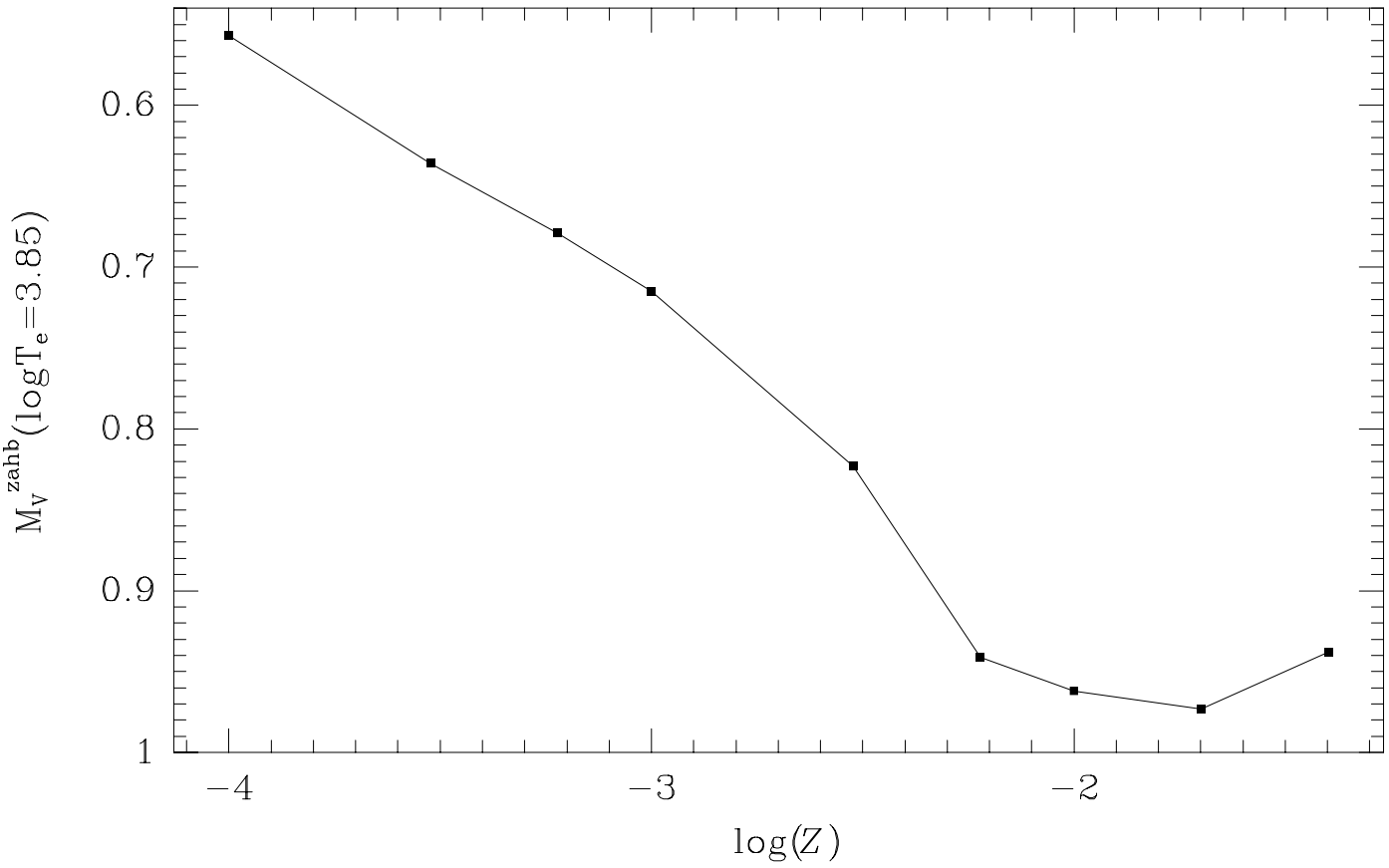
0.6
0.7
0.8
0.9
1
−4
−3
−2
log(Z)
$M_V^{zahb}(\log T_e=3.85)$

This figure "fig15.gif" is available in "gif" format from:

http://arXiv.org/ps/astro-ph/9609153v2